Current Topics in Biophysics 2010, 33 (suppl A), 87-93

EPR STUDY OF PHASE TRANSITIONS IN DMAAlS AND DMAGaS CRYSTALS

RYSZARD HRABAŃSKI[1], MONIKA JACKOWSKA[1], ZBIGNIEW CZAPLA[2]

[1]Institute of Physics, Czestochowa University of Technology, Al. Armii Krajowej 19, 42-200 Czestochowa, Poland, [2]Institute of Experimental Physics, University of Wroclaw, Plac Borna 8, 50-204 Wrocław, Poland

Received July 1, 2010; accepted August 18, 2010; published online November 20, 2010.

X-band electron paramagnetic resonance (EPR) investigations of Cr^{3+}-doped dimethylammonium aluminium sulphate hexahydrate (DMAAlS) and dimethylammonium gallium sulphate hexahydrate (DMAGaS) single crystals are presented in paraelectric and ferroelectric phase. Both crystal undergoes an order-disorder phase transition to ferroelectric phase at T_{C1}=152 K and T_{C1}=134 K, respectively. Additionally, DMAGaS shows at T_{C2} = 116 K a further first-order transition into an intermediate non-ferroelectric phase before it becomes antiferroelectric at T_{C3}= 60 K. The rotation patterns of the spectra show in the ferroelectric phase two chemically and magnetically equivalent Al and Ga sites in unit cell, which can be substituted by Cr^{3+} ions. The spin Hamiltonian parameters and the directions of the principal axes of the zero field splitting tensors have been determined and compare their values for the both crystals.

INTRODUCTION

The crystal structure of dimethylammonium aluminium sulfate hexahydrate (DMAAlS) $(CH_3)_2NH_2Al(SO_4)_2\cdot 6H_2O$ and the isomorphic gallium dimethylammonium sulfate hexahydrate (DMAGaS) is built up of Al or Ga cations coordinating six water molecules, regular SO_4 tetrahedra and $[(CH_3)_2NH_2]^+$ (DMA) cations, all hydrogen bonded into a three dimensional framework (Pietraszko, Lukaszewicz & Kirpichnikova, 1993). Both crystals are ferroelastic in the paraelectric phase, have the monoclinic space group $P2_1/n$, and exhibit an order-disorder type transition into a ferroelectric phase at T_{C1}= 152 K and T_{C1} = 134 K, respectively. Additionally, only DMAGaS shows at T_{C2} = 116 K a further first-order transition into an intermediate non-ferroelectric phase before it becomes antiferroelectric at T_{C3}= 60 K. The reason for this different behaviour of DMAAlS and DMAGaS is not yet fully understood. The ferroelectric transition is associated with the polar DMA cations, which execute hindered rotations in the ferroelastic phase and order partly in the ferroelectric phase. The intermediate phase seems to be modulated with tremendous disorder in the DMA cation system. Crystals of DMAAlS and DMAGaS have been widely studied using different experimental methods (Kapustianik, Fally, Kabelka & Warhanek, 1997; Dacko & Czapla, 1996; Kazimirov, Sarin, Smirnov & Shuvalov, 2004). In particular, magnetic resonance methods have already been employed in the studies of the phase transitions in both systems (Alsabbagh, Michel, Furtak & Czapla, 1998; Völkel, Alsabbagh., Böttcher, Michel, Milsch, Czapla & Furtak, 2000; Völkel, Böttcher, Czapla & Michel, 2002; Bednarski, Waplak & Kirpichnikova , 1999; Dolinšek, Klanjšek, Arčon , Kim Hae Jin, Seliger & Žagar, 1999; Völkel, Böttcher, Michel, & Czapla, 2003; Völkel, Böttcher, Michel, Czapla & Banys, 2005; Hrabanski, Janiec, Jackowska & Kapustianik, 2003; Hrabański, Janiec, & Kapustianik, 2004; Hrabański, Janiec-Mateja & Czapla, 2005; Hrabanski, Janiec-Mateja & Czapla, 2007). In the present paper we report the EPR measurements of chromium doped DMAAlS and DMAGaS performed in the X-band (~ 9.5 GHz) in the temperature range from room temperature (RT) down to liquid helium temperature. The rotation patterns of the spectra both in paraelectric, ferroelectric and antiferroelectric phases of both crystals are studied in detail and compared. The influence of the arrangements of the polar DMA units on the line shape of EPR spectra in the high temperature polar phase and low temperature non-polar phase is briefly discussed.

EXPERIMENTAL

Chromium-doped DMAAlS and DMAGaS single crystals were grown from aqueous solution containing 1 mol % $Cr_2(SO_4)_3\cdot 18H_2O$. The trivalent chromium ions with the electron configuration $3d^3$ substitute statistically at aluminium and gallium sites. The paramagnetic chromium ions are very sensitive probes on the slight changes of their environment.

EPR measurements were performed in the X-band (9.5 GHz) using standard spectrometers, equipped with a sample cavity of TE_{102} mode and 100 kHz modulations. Most of the spectra were recorded with the spectrometer, which was interfaced with a microcomputer via USB port for controlling the instrument, acquisition and display of the acquired spectra.

A goniometer sample holder provided the rotation of the sample (± 0.5°) about the given vertical axis. The cartesian laboratory xyz axes, chosen for the angle-dependent measurements were related to the **a**, **b**, **c** monoclinic crystallographic axes (Pietraszko et al., 1993) as follows: x || **a***, y || **b**, z || **c,** where **a*=b×c**.

The spectra were recorded by varying the orientation of the external magnetic field in a given plane at 5° angle intervals. The temperature of the sample was established by regulating the temperature of the cooling gas streaming around the sample, was controlled by Wildmad and Oxford Instrument cryostats with an accuracy of relative and absolute temperature values of 0.1 and 1 K, respectively.

RESULTS AND DISCUSSION

Angular dependences of the EPR spectra were studied at paraelectric phase and ferroelectric one in three planes perpendicular to the **a***-, **b**- and **c**-axes, respectively.

(a) (b)

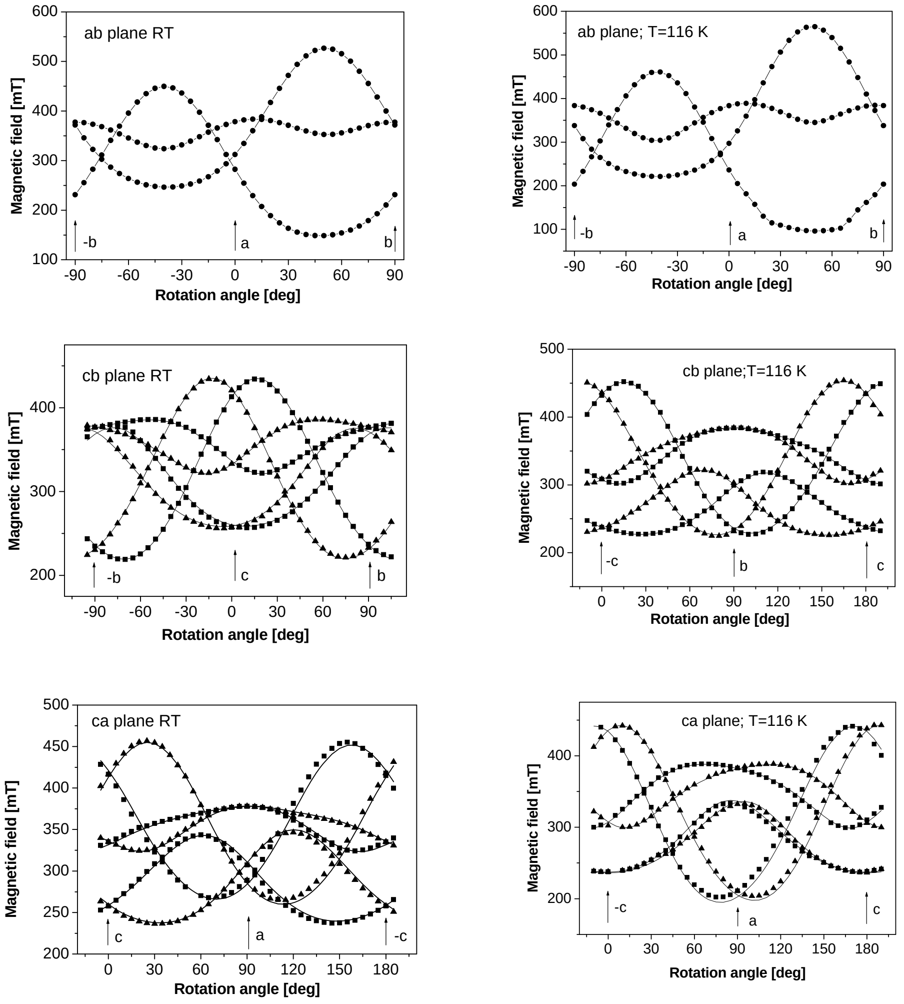

Fig. 1. The angular dependence of the Cr^{3+} EPR spectra in the paraelectric phase in DMAAlS at X-band: (a) in ferroelastic phase at RT and (b) in ferroelectric phase at 116 K. Closed circles and triangles represent the experimental data of two different sets of the fine structure lines. The solid lines show the fit result with the parameters given in table 1.

The rotation patterns taken in the ab, cb and ca planes for paraelectric and ferroelectric phases in DMAAlS are shown in Fig. 1. The rotation patterns of the spectra show in each phases of both crystals two structurally inequivalent sets of lines in accordance with two magnetically equivalent Al or Ga sites in the unit cell, which can be substituted by Cr^{3+} ions. For the each set, three allowed ($\Delta M_s = \pm 1$) and three quasi-forbidden transitions ($\Delta M_s = \pm 2$ and ± 3) between the four spin states 3/2, 1/2, -1/2 and –3/2, due to the effective spin quantum number S = 3/2, were clearly identified in the each plane. The quasi-forbidden transitions are not shown in the figures. The spectra can be described by the spin Hamiltonian (SH) (Rudowicz, 1987):

$$\hat{H} = \mu_B \mathbf{B} \cdot \mathbf{g} \cdot \mathbf{S} + \frac{1}{3}(b_2^0 O_2^0 + b_2^2 O_2^2) \qquad (1)$$

where **S** is the electron spin operator of the Cr^{3+} ion, μ_B is the Bohr magneton, **B** is the external magnetic field, **g** is the spectroscopic splitting tensor and the $b_n^m O_n^m$ terms represent zero field splitting contributions. The SH parameters were calculated with exact diagonalization of the energy matrices using computer program provided by Grachev (1998). In the literature the zero-field splitting parameters are often used D = b_2^0 and E = $b_2^2/3$. A procedure used for determination SH parameters was as follows. First, least-squares fittings were performed for each of the three planes studied yielding all b_n^m parameters (b_2^1, b_2^{-1}, b_2^{-2} have to be added for general orientation). The symmetric crystal field splitting tensor (usually **S·D·S** term in SH) can readily be identified with the b_n^m parameters through the following relations: $D_{xx}=(-1/3)(b_2^0 - b_2^2)$, $D_{zz} = (2/3)\ b_2^0$ $D_{yy}=(-1/3)(b_2^0 + b_2^2)$, $D_{xy} = (1/3)\, b_2^{-2}$, $D_{xz} = (1/6)\, b_2^1$, $D_{yz}= (1/6)\, b_2^{-1}$ (McGavin, 1987).

The matrix **D** was then diagonalized yielding the principal values of the fine-structure tensor D_{XX}, D_{YY}, D_{ZZ} and the direction cosines of principal axes X, Y, Z with respect to the laboratory the system x, y, z. The principal values of the fine structure tensor give the values of b_2^0 and b_2^2 parameters of SH (1). The procedure described above was used for analysis of the X-band results obtained in paraelectric and ferroelectric phases. The SH parameters determined in each phases are listed in table 1. There is a very good agreement between the experimental line positions and the theoretical ones calculated by the use of optimized SH parameters (Fig. 1).

Our experiments showed that no difference occurred between the fine structure parameters of two sites within the experimental errors for both system studied. The structural data indicates that six water molecules arranged in slightly disordered octahedral array surround each Cr^{3+} ion. The changes are seen both in the SH parameters and also in the positions of the principal axes of the zero field splitting tensor if we compare their values in both phases. The direction cosines of these tensors for DMAAlS crystal are given in table 2.

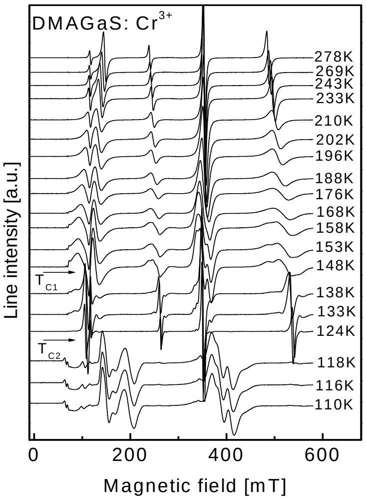

Fig. 2 Temperature dependence of the Cr^{3+} EPR spectrum in the DMAGaS measured at X-band with the magnetic field B in **bc** plane making an angle **(B,c)** = 30º. The phase transition temperatures T_{C1} and T_{C2} are shown.

The temperature dependence of EPR spectra was studied from RT down to liquid helium temperature. Fig. 2 shows the thermal evolution of the Cr^{3+} spectra in DMAGaS at selected orientation of the static magnetic field. Similarly as in DMAAlS, a strong broadening and then a line tripling is observed already in the ferroelastic phase far above phase transition. The satellites of these triplets disappear in the ferroelectric phase and lines narrow drastically on lowering the temperature. The appearance of triplets in the vicinity of ferroelectric phase transition in DMAGaS is clearly demonstrated in Fig. 3. Völkel et al (2000) gives a simple explanation of the observed line tripling taking into account the influence of four possible configuration of two neighbouring DMA groups on the water octahedron with the chromium probes substitution at the aluminium and gallium sites. Thus, the DMA groups have four equilibrium positions, which are realized in two groups with different probability. The alignment of the two neighbouring DMA cations influences the crystalline field which acts on the Cr^{3+} ion in center of water octahedron.

The structural environment of a Cr^{3+} probe site is schematically shown in Fig. 4. The two filled nitrogen positions *A*1-*B*1 mark a parallel configuration of the site. A Cr^{3+} probe can reside in any of the following four configurations: two DMA far (*A*2-*B*1), two DMA close (*A*1-*B*2), or twice one DMA close and one DMA far (*A*1-*B*1 or *A*2-*B*2). As already mentioned above, the realignment of the two neighboring dimethylammonium cations influences the crystalline field at the Cr^{3+} probe and leads to line shifts.

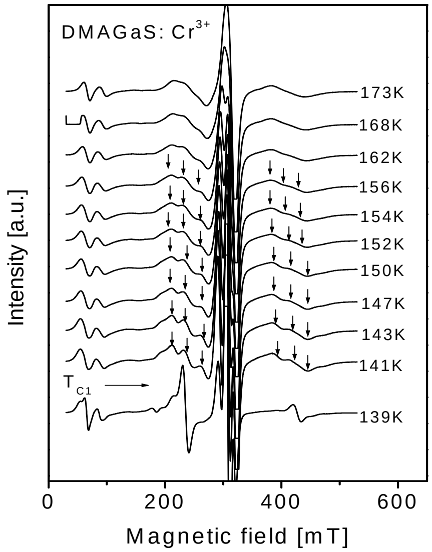

Fig. 3. Temperature dependence of the Cr^{3+} spectrum in DMAGaS near the phase transition into the ferroelectric phase measured at X-band with the magnetic field B in **ca** plane making an angle (**B**,**c**) = 50°. Arrows mark characteristic triplet lines.

Because the Cr^{3+} site is centro-symmetric in the paraelectric phase, in the ferroelectric phase the lines of the two inversion symmetric configurations *A*1-*B*1 and *A*2-*B*2 must collapse to one central line whereas the configurations *A*1-*B*2 and *A*2-*B*1 lead to the two satellites. The intensity ratio of the satellites to the central line

$$I_s/I_c=1/2(1-\eta^2)/(1+\eta^2) \tag{2}$$

is related to local order parameter (Völkel et al.,2000a)

$$\omega_1 - \omega_2 = \eta \tag{3}$$

of the DMA reorientation where $\omega_1=(1+\eta)/2$ and $\omega_2=(1-\eta)/2$ are the probabilities to find a DMA cation in the states 1 and 2, respectively, with $\omega_1+\omega_2$. The probability to find the antiparallel configurations A1-B2 or A2-B1 is then given by

$$\omega_1\,\omega_2=(1-\eta)^2/4) \tag{4}$$

whereas that to find the parallel ones, (A1-B1) and (A2-B2), is

$$\omega_1^2=(1+\eta)^2/4 \quad \text{and} \quad \omega_2^2=(1-\eta)^2/4 \tag{5}$$

respectively.

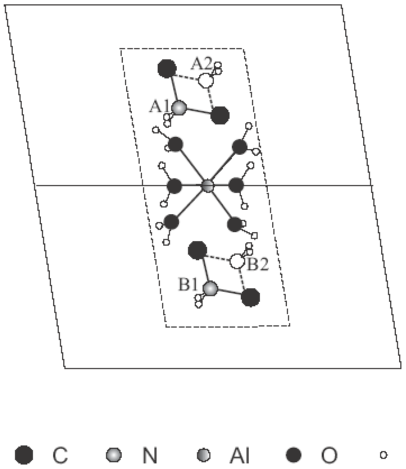

Fig. 4. A schematic representation of the dimethylammonium ion arrangements around an aluminium (gallium) or chromium water octahedron projected on the **a*b**-plane. Each of the two neighbouring dimethylammonium cations A and B can occupy one of the two polar positions 1 and 2. The shaded nitrogen positions correspond to the polar configuration A1–B1 (Völkel et al., 2000)

The combination of the equations (4) and (5) leads to the equation (2). The model describes properly the line intensity changes in the ferroelectric phase and allows for determination of the local order parameter of the DMA ordering. The validity of the model elaborated by Völkel et al. (2000) was experimentally verified also in our studies. With increasing order parameter the satellite intensity decreases. This behaviour of the spectra is also in good agreement with the four states model which was proposed for description of the phase transition crystals of DMAMeS (Me=Al, Ga) type by Stasyuk & Velychko (2001). The broadening of the lines and next their tripling confirm the order-disorder character of the ferroelectric phase transition. At T > T_{C1} DMA groups are dynamically disordered, executing random flips around the axis connecting the two methyl oxygens. Below T_{C1} the DMA molecule freeze out and the spontaneous dielectric polarization P_S occurs in the m-plane. Thus, the DMA group represents the basic reversible electric dipole and its ordering creates P_S below T_{C1}. The spectra in lower temperature part in Fig. 3 shows that at T_{C2} = 116 K the crystal undergoes another transition into the non-ferroelectric low temperature phase and the spectrum abruptly changes. It is associated with large shifts of line positions, striking line broadening and multiplication of the number of lines. These experimental findings are not in agreement with the assumption that at T_{C2} in DMAGaS crystals a transition into an antiferroelectric phase takes place. Völkel et al. (2003) have studied DMAGaS below T_{C2} = 116 K and explained the temperature behaviour of the spectra assuming the existence of a modulated phase in the crystal with commensurate regions and discommensurations before it becomes antiferroelectric at T_{C3} = 60 K. A modulation of the DMA order parameter has been postulated along the DMA–Ga$(H_2O)_6$–DMA direction (Völkel et al., 2005). The performed simulations have enabled to reproduce most of the characteristic spectrum changes in the intermediate phase and have shown that between 94 and 70 K a distinct commensurate phase occurs with a wave number equal ¼. However, in this case the line shape shows no edge singularity as usually observed in magnetic resonance experiments for incommensurately modulated crystals because the DMA order parameter is associated with changes of the line intensities and not with changes of line positions. Fig. 5 shows the temperature dependence of the Cr^{3+} spectra in DMAGaS at a selected orientation of the static magnetic field in the temperature range from 75 to 40 K. Unusual changes of the spectra in the intermediate phase are observed, namely, doubling of the number of lines and their broadening. With lowering temperature, the lines positions of almost do not change but they narrow remarkably. In the antiferroelectric phase, there is no symmetry reason for collapsing of lines as observed in the para- and ferroelectric phase. Each Cr^{3+} can be found at one in four structural configurations formed by the different arrangement of the two neighbouring DMA cations. The slightly different structural environment of the Cr^{3+} ions results in a different fine structure splitting.

The concepts which described above may be extended to the antiferroelectric case (Völkel et al., 2005). In the low-temperature phase, there is no symmetry reason for collapsing of lines anymore. Therefore, for each Cr^{3+} site a line quartet is expected instead of a triplet. Additionally, we have to take into consideration the doubling of the unit cell. The spectra of formerly identical sites in neighboring unit cells e.g., Ga sites (0, 0.5, 0) and (0, 1.5, 0) become now different. Consequently, we have to model the observed line shapes in the low-temperature phase by means of two quartets. The intensities of the quartet lines are again related to the local order parameter η. Let us now denote the occupancy probabilities for the DMA orientations presented in Fig. 4 as ω_{A1} , ω_{A2} , ω_{B1}, and ω_{B2}. In the ferroelectric case discussed above the probability for finding the neighboring DMA molecules at left or right position is $\omega_{A1}= \omega_{B1}=\omega_1$ and $\omega_{A2}= \omega_{B2}= \omega_2$, respectively. If we assume that the DMA molecules show an antiferroelectric order along the crystallographic **b** axis, the antiparallel aligned neighboring DMA cations must have equal occupancy probability leading to $\omega_{A1}= \omega_{B2}= \omega_1$ and $\omega_{A2}= \omega_{B1}= \omega_2$. The order parameter is defined in the same manner as above. However, the probability to find the antiparallel configurations *A*1-*B*2 and *A*2-*B*1 is now given by ω_1^2 and ω_2^2, respectively, whereas the parallel configurations *A*1-*B*1 or *A*2-*B*2 exist both with the same probability $\omega1 \cdot \omega2$. The intensity ratio of the two outer lines to the middle one's is then given by
$r_1= (1+ \eta)/(1- \eta)$ and $r_2= (1- \eta)/(1+ \eta)$, respectively. It means that in the antiferroelectric state with $\eta \approx 1$ only one of the outer lines of the quartets is observable in agreement with the experimental results. We have also to take into consideration the doubling the unit cell. In consequence the spectrum is expected to consist of two overlapping quartets where the intensities are given by the statistical weights of the configurations. In the totally ordered antiferroelectric phase only one intense doublet remains. On the other hand, it should be noted that the EPR spectra of chromium doped DMAAlS do not show any changes at lower temperatures, besides the anomaly linked to the ferroelectric phase transition similar to that observed in DMAGaS. Only small line shifts are observed down to the lowest temperatures.

Table 1. Spin-Hamiltonian parameters for Cr^{3+} in paraelectric (RT) and ferroelectric phases of DMAAlS and DMAGaS. Zero field splitting parameters are in 10^{-4} cm^{-1}.

Crystal	Temperature	g	b_2^0	b_2^2
DMAAlS	RT	1.980±0.003	950±15	198±10
	108 K	1.980±0.005	1133±15	214±10
DMAGaS	RT	1.982±0.002	890±15	386±15
	125 K	1.982±0.002	1088±15	39±15
	40 K	1.976	1425	1120

Table 2. Direction cosines of I and II site of Cr^{3+} ions in DMAAlS at RT.

Site	Principal axes of the complex	Direction cosines		
		x	y	z
I, II	X_I, X_{II}	±0.385	±0.555	0.738
	Y_I, Y_{II}	0.673	±0.378	±0.635
	Z_I, Z_{II}	0.631	0.740	±0.228

One has to note that in the studied temperature range in both crystals the DMA molecule configuration is not static but highly dynamic. The DMA molecules execute fast rotational reorientations with frequencies slowing down about thousand times with lowering temperature from RT to 40 K in DMAGaS (Völkel et al., 2003;

Hrabanski et al., 2007). The linewidth changes may be treated as a measure of the reorientation rate of the DMA molecules for the temperature interval between 70 K and 40 K. For this temperature range we can assume that the line broadening is mainly caused by the reorientation. It is well known that dielectric data obtained for low temperature phase of DMAGaS show that the polarization reorientation is several order of magnitude slower.

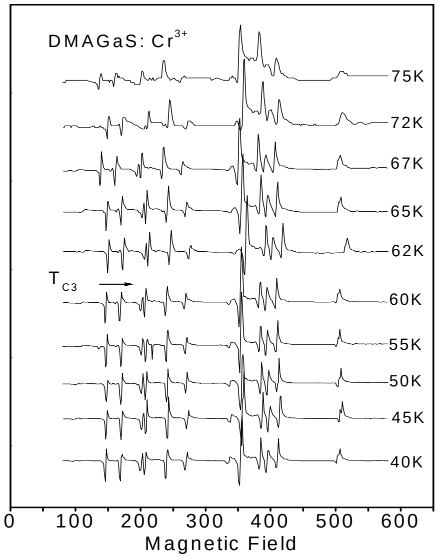

Fig. 5. Temperature dependence of the Cr^{3+} spectrum in DMAGaS near the phase transition into the antiferroelectric phase measured at X-band with the magnetic field **B** in bc plane making an angle (**B**,**c**) = 15°

Völkel et. al., 2005 has showed that all these complex experimental findings can be qualitatively understood in a very consistent manner within the semimicroscopic extended DIFFOUR model. Qualitatively, the extended DIFFOUR model provides phase diagrams, which give a consistent description of the phase sequences, observed experimentally. The model is based on the chain-like structure in the form of the $–DMA_{(i)}–Ga/Al(H_2O)_{6(i)}–DMA_{(i+1)}–Ga/Al(H_2O)_{6(i+)}$-chains where the DMA molecules represent the orientable electric dipoles. The model gives also indications that the different behaviour of the crystals DMAAlS and DMAGaS originates in different interaction strengths between the DMA dipoles mediated by the $Ga(H_2O)_6$ and $Al(H_2O)_6$ octahedrons. In order to complete the model description of this crystal family, further experimental studies of the DMAAlS/DMAGaS mixed crystals should be carried out and quantitative calculations of the phase diagram should be performed.

REFERENCES

Pietraszko A., Lukaszewicz K. & Kirpichnikova L.F., (1993). Crystal structures of $(CH_3)_2NH_2Al(SO_4)_2{\cdot}6H_2O$, $(CH_3)_2NH_2Ga(SO_4)_2{\cdot}6H_2O$ and $(CH_3)_2NH_2Al(S_{0.89}Se_{0.11}O_4)_2{\cdot}6H_2O$, *Polish J. Chem.* **67**, 1877-1884.

Kapustianik V., Fally M., Kabelka H. & Warhanek H. (1997). Anomalous dielectric behaviour of $(CH_3)_2NH_2Al(SO_4)_2{\cdot}6H_2O$ crystals in the ferroelectric phase, *J. Phys. Condens. Matter* **9**, 723-733.

Dacko S. & Czapla Z., (1996). On the phase transitions in DMAAS and DmaGS, *Ferroelectrics,* **185**, 143-148

Kazimirov V.Yu., Sarin V.A., Smirnov M.B. & Shuvalov L.A., (2004). Investigation of ferroelectric phase transition in DMAAS Crystals: Neutron diffraction, Neutron spectroscopy, theoretical model, *Ferroelectrics* **299**, 59-73.

Stasyuk I.V. &. Velychko O.V, (2001). Order-disorder model of phase transitions in the DMAGaS-DMAAlS family crystals, *Phase Transitions* **73**, 483-495.

Alsabbagh N., Michel D., Furtak J.& Czapla Z. (1998). ^{27}Al and ^{71}Ga NMR Measurements on single crystals of DMAAS and DMAGaS, *Phys. Stat. Sol. A* **167**, 77-87.

Völkel G., Alsabbagh N., Böttcher R., Michel D., Milsch B., Czapla Z. & Furtak J., (2000). Local order-disorder behaviuor in Cr^{+3} doped dimethylammonium aluminum sulfate hexahydrate (DMAAS) studied by electron paramagnetic resonance, *J. Phys. Condens. Matter* **12**, 4553-4566

Völkel G., Böttcher R., Czapla Z. & Michel D., (2002). EPR studies of chromium doped dimethylammonium gallium and aluminum sulfate hexahydrate (DMAGaS and DMAAS), *Ferroelectrics,* **268**, 181-186.

Bednarski W., Waplak S. & Kirpichnikova L.F., (1999). The mechanism of the phase transition in $(CH_3)_2NH_2Al(SO_4)_2{\cdot}6H_2O$ studied by EPR of Cr^{3+}, *J. Phys. Condens. Matter* , **11,** 1567-1574.

Dolinšek J., Klanjšek M., Arčon D., Kim Hae Jin, Seliger J. & Žagar V., (1999), ^1H and ^{27}Al NMR study of the ferroelectric transition in dimethylammonium aluminum sulphate hexahydrate $(CH_3)_2NH_2Al(SO_4)_2{\cdot}6H_2O$, *Phys. Rev. B* **59**, 3640-3667

Völkel G., Böttcher R., Michel D., & Czapla Z., (2003) Low-temperature phase of chromium doped dimethylammonium gallium sulfate hexahydrate studied by electron paramagnetic resonance, *Phys. Rev. B* **67**, 241111-241114

Völkel G., Böttcher R., Michel D., Czapla Z. & Banys J., (2005). Dimethylammonium gallium sulfate hexahydrate and aluminum sulfate hexahydrate –members of a crystal family with exceptional commensurate/in commensurate phase sequences, *J. Phys.Condens. Matter* **17,** 4511-4529.

Hrabanski R., Janiec M, Jackowska M. & Kapustianik V., (2003). EPR study of the order-disorder phase transition in DMAAS crystal, Ferroelectrics, **291**, 241-249

Hrabański R., Janiec M., & Kapustianik V., (2004). EPR study of the ferroelectric phase transition In chromium doped DMAAS, *Appl. Magn. Reson.* **27**, 19-27

Hrabański R., Janiec-Mateja M., & Czapla Z., (2005) EPR study of the phase transition -n dimethylammonium pallium sulphate hexahydrate, *Acta Phys. Pol.* **108**, 283-290.

Hrabanski R, Janiec-Mateja M. & Czapla Z., (2007) EPR study of local ordering in DMAAl and DMAGaS, *Phase Transitions*, **80**. 163-169.

Rudowicz Cz. (1987), Concept of spin hamiltonian, forms of zero field splitting and electronic zeeman hamiltonians and relations between parameters used in EPR. A critical review, Magn. Res. Rev., **13**, 1-89

McGavin D.G. (1987), Symmetry Constrains on EPR spin Hamiltonian Parameters, J. Magn. Res., **74**, 19-55,

Grachev V.G. (1998), *Visual EPR program v. 2.08*, Osnabrück: Fachbereich Physik, Universität Osnabrück.